Heliyon 10 (2024) e34317

Contents lists available at ScienceDirect

Heliyon

journal homepage: www.cell.com/heliyon

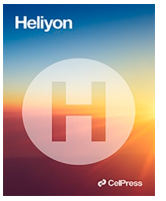

Research article

The combination of exon sequencing and metabolomics to establish a molecular typing system for gastric cancer

Shanshan Yu [a,1], Ming Chen [b,1], Xiaohua Zhu [c,1], Cheng Chen [a], Jinxiao Liang [a], Haiyong Wang [a], Jun Lu [a], Yongfeng Ding [d], Mei Kong [e], Lisong Teng [a], Donghui Zhou [a,*]

[a] Department of Surgical Oncology, The First Affiliated Hospital, Zhejiang University School of Medicine, Hangzhou, 310003, China
[b] Department of Surgical Oncology, Children's Hospital, Zhejiang University School of Medicine, Hangzhou, 310052, China
[c] Department of Medical Oncology, Shaoxing People's Hospital, Shaoxing, 312000, China
[d] Department of Medical Oncology, The First Affiliated Hospital, Zhejiang University School of Medicine, Hangzhou, 310003, China
[e] Department of Pathology, The First Affiliated Hospital, Zhejiang University School of Medicine, Hangzhou, 310003, China

ARTICLE INFO

Keywords:
Gastric cancer
Heterogeneity
Molecular classification
Whole-exome sequencing
Metabolic dysregulation

ABSTRACT

Background: Gastric cancer (GC) is one of the most common malignant tumors in the world. It has become increasingly difficult to meet the needs of precision therapy using the existing molecular typing system. Therefore, developing a more effective molecular typing system for GC is urgent.
Methods: In this study, 100 Chinese GC patients were included. Whole-exome sequencing (WES) and metabolomics analysis were performed to reveal the characteristics of genomic and metabolic changes.
Results: In WES, nonsynonymous mutations accounted for the majority. Based on metabolomics, GC has been divided into three subtypes with distinct metabolic features. Importantly, we ultimately divided GC into four subtypes with different metabolic characteristics, genomic alterations, and clinical prognoses by incorporating biomics analysis.
Conclusions: Integrating biological features, we constructed a novel molecular system for GC that was closely related to genetics and metabolism, providing new insights for further understanding the heterogeneity and formulating precise treatment strategies.

1. Introduction

Gastric cancer (GC) is one of the most common malignant tumors in the world. According to the latest data, GC is the third most malignant tumor in China [1]. The current clinical treatment model for GC has gradually changed from a single treatment model to a comprehensive individual treatment model. However, due to hidden early symptoms and other reasons, the 5-year survival rate of GC is only 35.9 % [2]. More importantly, GC is a highly heterogeneous tumor involving histopathological, genetic, epigenetic and transcriptomic aspects [3], which poses serious challenges for accurate diagnosis and personalized treatment. Therefore, the lack of effective prediction markers for screening out the eligible groups is the bottleneck restricting the progress of clinical research on GC.

* Corresponding author. Department of Surgical Oncology, The First Affiliated Hospital, School of Medicine, Zhejiang University, Hangzhou, China.
E-mail address: 1193076@zju.edu.cn (D. Zhou).
[1] These authors have contributed equally to this work.

https://doi.org/10.1016/j.heliyon.2024.e34317
Received 22 November 2023; Received in revised form 8 July 2024; Accepted 8 July 2024
Available online 9 July 2024

Over the past few decades, efforts have been made to classify GC into several subtypes to guide treatment decisions. Although histopathological classification has certain reference value in treatment decision-making and prognosis prediction, traditional classification can no longer meet the needs of individualized treatment. This demand has spawned the TCGA classification [3]. However, TCGA typing does not consider the relationships between subtypes, efficacy, and prognosis due to the lack of sufficient clinical follow-up data. Additionally, most of its specimens were taken from patients in Europe and America, which has limited guidance value for East Asia. China, a country with a large number of individuals affected by stomach cancer, needs to include enough clinical samples urgently to improve GC molecular typing methods suitable for Chinese people.

In recent years, the rapid development of high-throughput second-generation sequencing technology has made it possible to accurately classify GC molecule typing. The advent of WES successfully described the molecular basis of disease diversity phenotypes [4–6]. Recent studies have attempted to perform the molecular typing of GC based on gene mutations and other levels. For example, in combination with genomic hybridization and expression microarray analysis of gastric cancer, Tay et al. divided GC into three categories, namely, tumorigenic, reactive and gastro-like, showing significant prognostic differences among these types [7]. In addition, our research group previously divided gastric cancer among Chinese patients into four subtypes with different clinical phenotypes and prognoses by integrating multidimensional genomic characteristics [8]. The above studies are of great significance for revealing the full picture of GC genome variation, understanding the pathogenesis of GC and guiding research on precision treatment.

Gastric cancer is a malignancy formed by the long-term interactions of internal and external pathogenic factors. WES can reveal changes at the gene level, which is of certain value for the understanding of disease mechanisms and providing clinical drug guidance. However, nongenetic factors are also key determinants in disease occurrence and development. As an emerging omics research technology, metabolomics can provide all the metabolic profile information for a specific tumor to understand the characteristics of the disease phenotype [9]. Thus, multiomics tumor analysis provides a new window to identify molecular disease drivers, leading to more precise drug therapies [10].

In this study, we conducted whole-exon sequencing and metabolomics analysis on 100 GC tissue samples and paired paracancerous tissues. Based on the metabolic profile data of cancer tissues, we preliminarily established a new molecular typing system for GC. Considering the high gene mutation rate of gastric cancer, we further combined WES to establish the first novel molecular system based on biomics in China, in which we divided GC into four subtypes that show significant differences in clinical and molecular characteristics. This study investigated the pathological mechanisms that enrich the occurrence and development of gastric cancer and provided a theoretical basis for the identification of subtypes and potential targeted drug therapy.

2. Results

2.1. Clinicopathologic features of patients

In a cohort of 100 gastric cancer patients independently confirmed by at least two experienced pathologists, we found that the

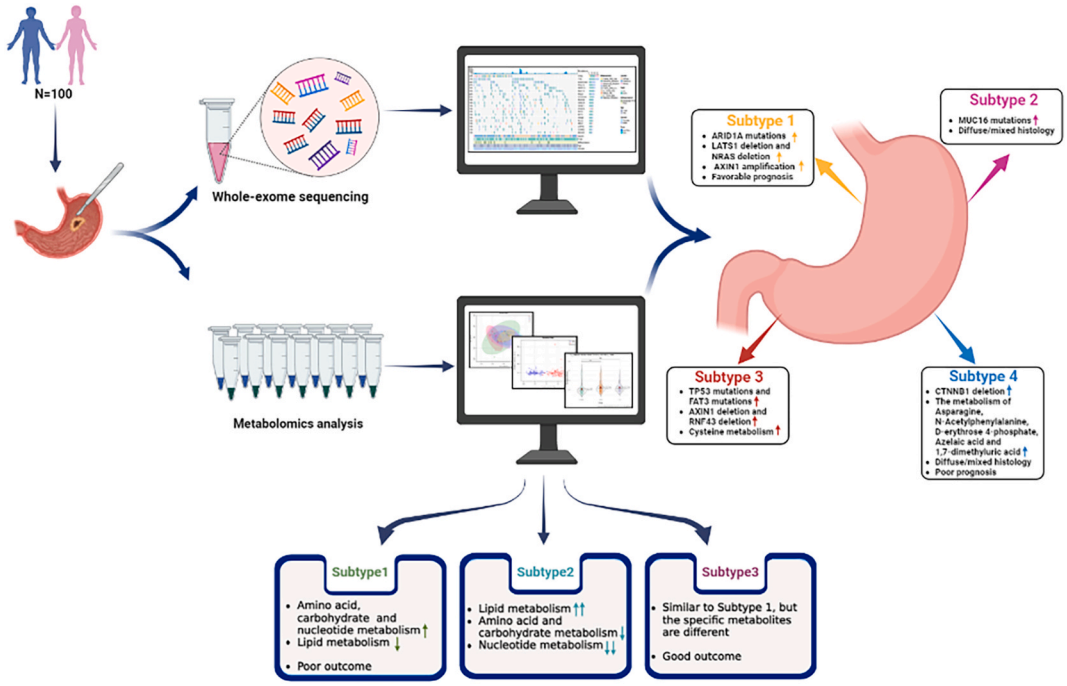

Fig. 1. Schematic overview of the study design.

patients in this cohort ranged in age from 27 to 82 years, including 71 males and 29 females and 10, 24, 59 and 7 cases for stages I/II/III/IV, respectively. The median follow-up time was 48 months. Fifty patients (50 %) developed recurrence and metastasis, 50 patients (50 %) survived, and 48 patients (48 %) died (Table S2).

2.2. Overview of molecular mutations in gastric cancer

2.2.1. Somatic mutant spectrum

To comprehensively analyze the molecular characteristics and metabolic differences of GC tumors, multiple omics analyses were performed on 100 patient-paired tumor and paracancerous tissues samples, including WES and metabolomics analysis (Fig. 1). In the WES results, the sequencing depths of gastric cancer tissue and normal tissue were 227 times and 125 times, respectively (Table S3). According to the WES results, a total of 17,984 somatic mutations were identified, with nonsynonymous mutations accounting for the dominant proportion (16,940, 94.2 %) (Table S4). A waterfall diagram was constructed to visualize the top 20 genes with mutation ratios, which included *TP53*, *TTN*, *ANKRD36C*, *MUC16*, and *NBPF10* (Fig. 2a). The mutation distributions of *TP53*, *TTN*, *MUC16*, and *NBPF10* are shown in Figs. S1a–1d. We also compared the major somatic mutation genes in TCGA and found that the mutation frequencies of most of the genes remained consistent, but there were differences in the mutation frequencies of some genes (Fig. 2b–Table S5). This difference may be due to the fact that TCGA classification is based on European and American populations, small sample sizes, or individual differences. The rates of mutation for *TP53,* one of the genes with the highest mutation frequency, were found to be different between intestinal tumors and diffuse/mixed tumors, while no other gene mutation rates were found to be different between other clinicopathologic subtypes (Fig. 2c–Table S6). In addition, by analyzing the patterns of base replacement, we found that the incidence of base transversion was higher than that of base transition, reflecting a large bias in this result (Fig. 2d). In addition, a 96-substitution classification method was used to characterize and identify the mutation characteristics and types of genome mutations, and three independent mutation signatures were matched (Fig. 2e). Collectively, an unsupervised clustering was used to divide GC into three subtypes based on the somatic mutant spectrum. Survival analysis revealed that subtype 1 had the better prognosis and subtype 3 had the poor prognosis (Figs. S1e–g). COX regression based on Sig_Cluster revealed a trend consistent with the survival curve. TNM stage and type were independent prognostic factors, while no differences between subtypes were identified in the other pathological data (Table S7, Fig. S1h).

2.2.2. Somatic copy number variants (CNVs) and changes in genomic signaling pathways

The characteristics of CNVs were then analyzed. Sixty-five significant CNVs were identified by GISTIC 2.0, with 24 amplified and 41 missing. The amplified CNVs included a large number of proto-oncogenes, such as *CCNE1* (19q12), *ERBB2* (17q12), *CCND1* (11q13.3) and *MYC* (8q24.21), and the missing CNVs included a large number of tumor suppressor genes, such as *ARID1A* (1P3.11), *MLH1* (3p21.31), and *PTEN* (10q23.31) (Fig. 2f–g, Table S8). According to the characteristics of CNVs, the samples were divided into two subtypes by unsupervised clustering. The prognostic analysis revealed that the overall survival (OS) of subtype 1 was poor (Figs. S2a–c). Cox regression analysis based on CNV typing demonstrated that TNM stage could be used as an independent prognostic factor (Fig. S2d, Table S9). Subsequently, KEGG was used to analyze somatic mutation and CNV characteristics and revealed the changes in tumor-related signaling pathways in GC tissues. The top 4 pathways included the well-known RTK-RAS, Notch, Wnt and Hippo signaling pathways (Fig. S3). In addition to the well-known target *NTRK2, DLL4* amplification, *NOTCH4* deletion, and *CTNNB1* deletion were all identified as potential therapeutic targets.

2.2.3. Neoantigen analysis and multidimensional genomic characteristics revealed the molecular subtypes of GC

The advent of immunotherapy has opened a new chapter in the comprehensive treatment of GC and prompted our curiosity about the presentation patterns of neoantigens in 100 GC tissues. We found that a total of 16,342 predicted neoantigens were identified in 100 patients, with the numbers of neoantigens per patient ranging from 0 to 1283, reflecting large individual differences (Table S10). In addition, 2266 (13.87 %) neoantigens were predicted to have affinity with HLA-A*11:01 (Fig. 2h–Table S11), and a positive correlation was found between the number of neoantigens and tumor mutation burden (TMB) ($R^2 = 0.25$, $p = 1.398577e\text{-}07$, Fig. 2i). By further exploring the landscape of predicted neoantigens and somatic mutations, we found that neoantigens were mainly derived from somatic mutations of the mucin (MUC) family, among which the proportions were 19 % for *MUC16,* 13 % for *MUC12* and 11 % for *MUC4* (Table S12), suggesting that the MUC family might guide the correct implementation of immunotherapy for GC. Following the above analyses, GC was divided into two subtypes by unsupervised cluster analysis. Regrettably, there was a large difference in sample size and a lack of prognostic analysis (Fig. S4). Clinicopathological correlation analysis revealed no relevant pathological features (Table S13). By combining the somatic mutation characteristics, CNV, predicted neoantigens and important tumor-related gene changes, 100 GC samples were ultimately divided into two subtypes. (Fig. S5a). Subsequently, survival analysis found that subtype 1 had poor survival (PFS) (Figs. S5b–c). Cox regression analysis showed that TNM stages and types could be used as independent prognostic factors (Fig. S5d), while no differences among subtypes were found in the other pathological data (Table S14). The significant mutated genes among the subtypes of the molecular typing system established based on integrated genomic characteristics are shown in Table S15.

2.2.4. The metabolic profile reflected metabolic dysregulation in GC

Sample stability was tested by principal component analysis (PCA), and the results showed that there was little difference between samples of each batch and that the samples were stable (Fig. 3a). The coefficient of variation (CV) was further used for testing, and the results showed that the average CV of each batch was within 30 %, indicating that each batch had good stability (Table S16). Then,

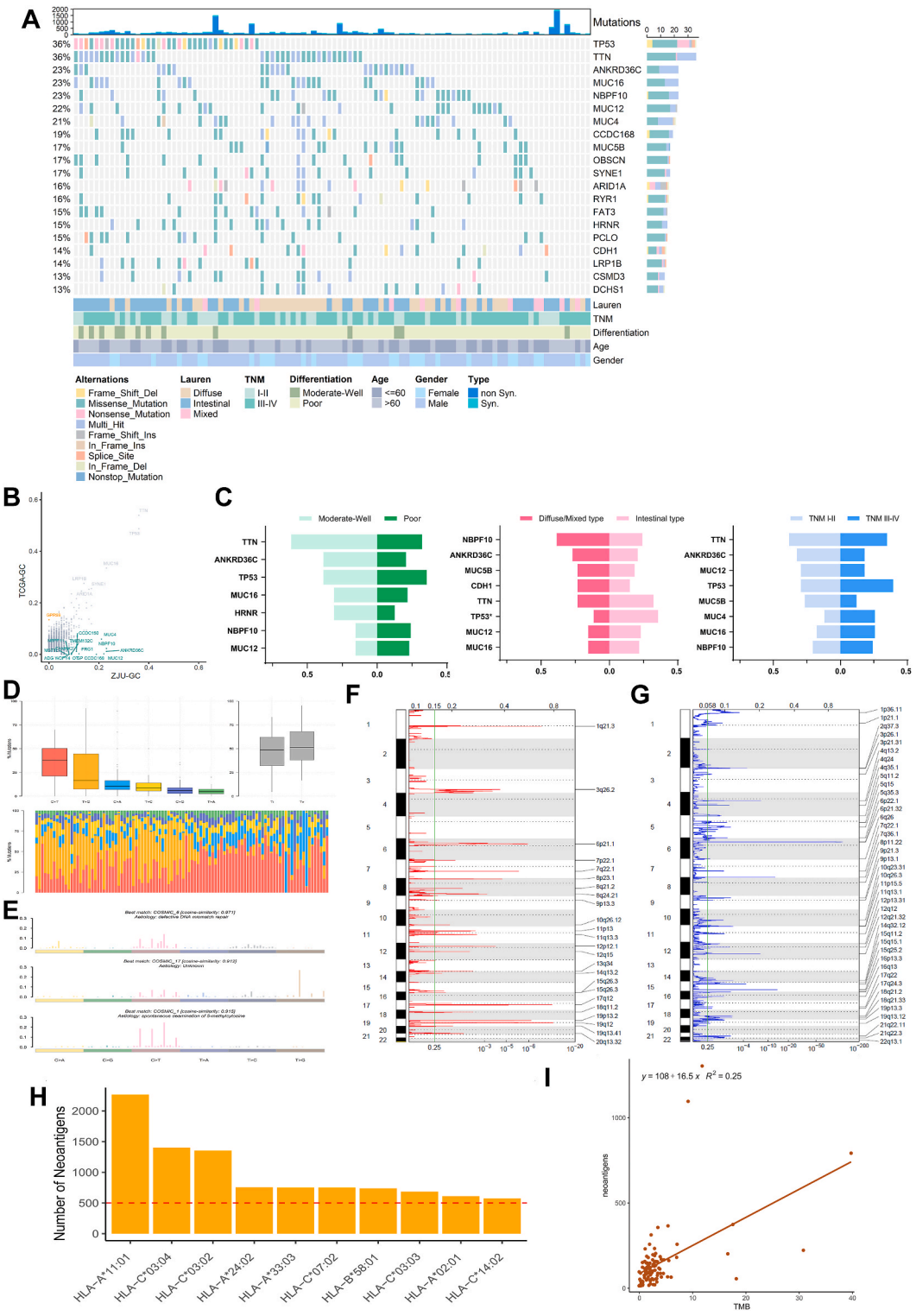

Fig. 2. Landscape of whole-exon sequencing of the 100 gastric cancer samples in the ZJU-GC cohort.
a. Somatic mutation waterfall diagram showing the top 20 genes with their mutation ratios, along with an intermediate matrix by gene (row) and sample (column). b. Comparison of the mutation rates between this cohort and the TCGA-GC gene cohort. The blue and orange dots represent genes with higher and lower mutation rates, respectively. c. Comparison of the gene mutation rates of different clinicopathologic subtypes. d. Diagram of 6-base replacement modes. Ti represents transition, and Tv represents transversion. e. Characterization and identification of the genomic features in this cohort. Mutation characteristics are represented according to the 96-substitution classification. The 96-substitution classification mutation types

are displayed on the horizontal axis, and the frequency of each mutation type is displayed on the vertical axis. f. Significant CNVs with amplifications identified by GISTIC 2.0. g. Significant CNVs with deletions identified by GISTIC 2.0. h. Predicted binding sites of neoantigens. i. Correlations between TMB and neoantigens in the 100 samples. (For interpretation of the references to color in this figure legend, the reader is referred to the Web version of this article.)

OPLS-DA analysis revealed the heterogeneity within the cancer tissue group was higher than that within the PT group (Fig. 3b). The reliability of the model was verified by permutation testing, indicating the good fitting accuracy of the OPLS-DA model (Fig. 3c). Subsequently, through Euclidean distance analysis, we again confirmed that the heterogeneity between gastric cancer tissues, gastric cancer tissues and normal tissues was significantly higher than that between normal tissues, unveiling the heterogeneity of gastric cancer from the metabolomics perspective (Fig. 3d).

Further analysis was performed to screen out key differential metabolites between cancerous and paracancerous tissues. As shown in the S-plot of OPLS-DA, a total of 70 differential metabolites were screened out according to the standard that Variable Importance for the Projection (VIP) is > 1 (Fig. 3e–Table S17), whose distribution was visualized by constructing a volcano map (Fig. 3f). The Mann–Whitney test was then performed to examine the expression levels of fatty acids and triglycerides (TGs) in cancerous and paracancerous tissues. The results showed that the expression levels of fatty acid metabolites such as arachidonic acid, and eicosatrienoic acid, were significantly higher in cancer tissues than in paracancerous tissues (Fig. 3g–k, $p < 0.001$). The expression levels of TG (42:2), TG (44:3), TG (46:3) and TG (52:14) in cancer tissues were also significantly higher than those in paracancerous tissues (Fig. 3l–o, $p < 0.0001$), which was consistent with the results shown in the heatmap (Fig. 3p).

Inspired by the high expression levels of fatty acids and TGs in cancer tissues, we also wanted to know the pathway enrichment results of the differential metabolites. The results showed that the enriched metabolic pathways were mainly concentrated in the upregulated metabolites in cancerous tissues. Several metabolic pathways, such as D-glutamine and D-glutamate metabolism, showed strong disturbances among the upregulated metabolites in cancer tissues (Fig. 3q).

In addition, we analyzed the different metabolites among different types of GC tissues based on different clinicopathological features, such as diffuse and intestinal GC (Fig. S6a), poorly and moderately differentiated GC (Fig. S6b), signet ring cell carcinoma (SRCC) and gastric adenocarcinoma (Fig. S6c), and stages I-II and III-IV GC (Fig. S6d). Tables S18–S21 show the corresponding differential metabolites.

2.2.5. The molecular typing system of GC was established based on metabolomics

To reveal the metabolic heterogeneity of GC, unsupervised cluster analysis was performed using the NMF method, in which cophenetic, dispersion, evar, residuals and rss were used as cluster evaluation indicators to predict the optimal rank value (Fig. 4a). Taking the first point with the largest change in cophenetics as the judgment criterion, we determined that the best rank value was 3 (Fig. 4b). Based on the classification number of the 3 types, unsupervised clustering were conducted to draw the consensus matrix, which revealed that there were obvious differences among the 3 subtypes (Fig. 4c). Clinicopathological features were included in the construction of the heatmap. There were 27 cases of Cluster 1, 52 cases of Cluster 2 and 21 cases of Cluster 3 (Fig. 4d). By further analyzing the correlations between different subtypes and histopathology, we realized that Cluster 1 had higher proportion of stage III-IV samples and poorly differentiated samples, while Clusters 2 and 3 had certain similarities in clinicopathological characteristics (Fig. 4e–i). Survival analysis revealed that Cluster 1 had the worst prognosis, which was consistent with its clinical characteristics (Fig. 4j). Cox regression analyses revealed that TNM staging was an independent risk factor for the prognosis of GC ($p = 0.001$). At the same time, consistent with the clinical survival analysis, the risk ratio (HR) of Cluster 2 was much lower than that of Cluster 1, which indicated that the classification system was an independent prognostic factor (Fig. 4k-l).

2.2.6. Different metabolic subtypes showed distinct metabolic characteristics

Next, we determined whether different metabolic subtypes had unique metabolic features. Similar to the previous method, we screened differential metabolites of different clusters (Fig. S7a, Table S22, Fig. S7c, Table S23, Fig. S7e, Table S24). Then, according to Cluster 1 vs. Clusters 2 & 3 enrichment pathway analysis, several metabolic pathways, such as tyrosine metabolism and proline metabolism, exhibited strong disturbances in the upregulated metabolites of Cluster 1. Thiamine metabolism and methionine metabolism showed strong changes in downregulated metabolites of the Cluster 1 subtype (Fig. S7b). According to Cluster 2 vs. Clusters 1 & 3 enrichment pathway analysis, in the Cluster 2, the metabolic disturbance pathway was mainly concentrated in downregulated metabolites, such as tyrosine metabolism and vitamin B6 metabolism. According to Cluster 3 vs. Clusters 1 & 2 enrichment pathway analysis, in Cluster 3, the metabolic disturbance pathway was mainly focused on upregulated metabolites, such as histidine metabolism and caffeine metabolism (Fig. S7f). A heatmap was then drawn according to the metabolic characteristics of each subtype. The results showed that Cluster 1 was characterized by high levels of amino acid, carbohydrate and nucleotide metabolites but low levels of lipid metabolism. Clusters 3 and 1 were similar, but the specific metabolites were different. Compared with Clusters 1 and 3, Cluster 2 had very high levels of lipid metabolites and energy metabolism and low levels of amino acid and carbohydrate metabolism and nucleotide metabolites (Fig. 5a). An overview map of metabolic pathways, including carbohydrate metabolism, amino acid metabolism, fatty acid biosynthesis and lipid metabolism, was drawn based on the characteristics of the three subtypes. Phosphatidyl ethanolamine in lipid metabolism of the Cluster 1 subtype was significantly downregulated, the overall level of lipid metabolism was relatively low, and amino acid synthesis was upregulated. Amino acid metabolism and the tricarboxylic acid cycle were generally downregulated in the Cluster 2 subtype. Histidine synthesis and myristic acid synthesis were obviously accumulated in the Cluster 3 subtype (Fig. 5b). In addition, the expression levels of typical metabolites and lipids among the three subtypes showed that the

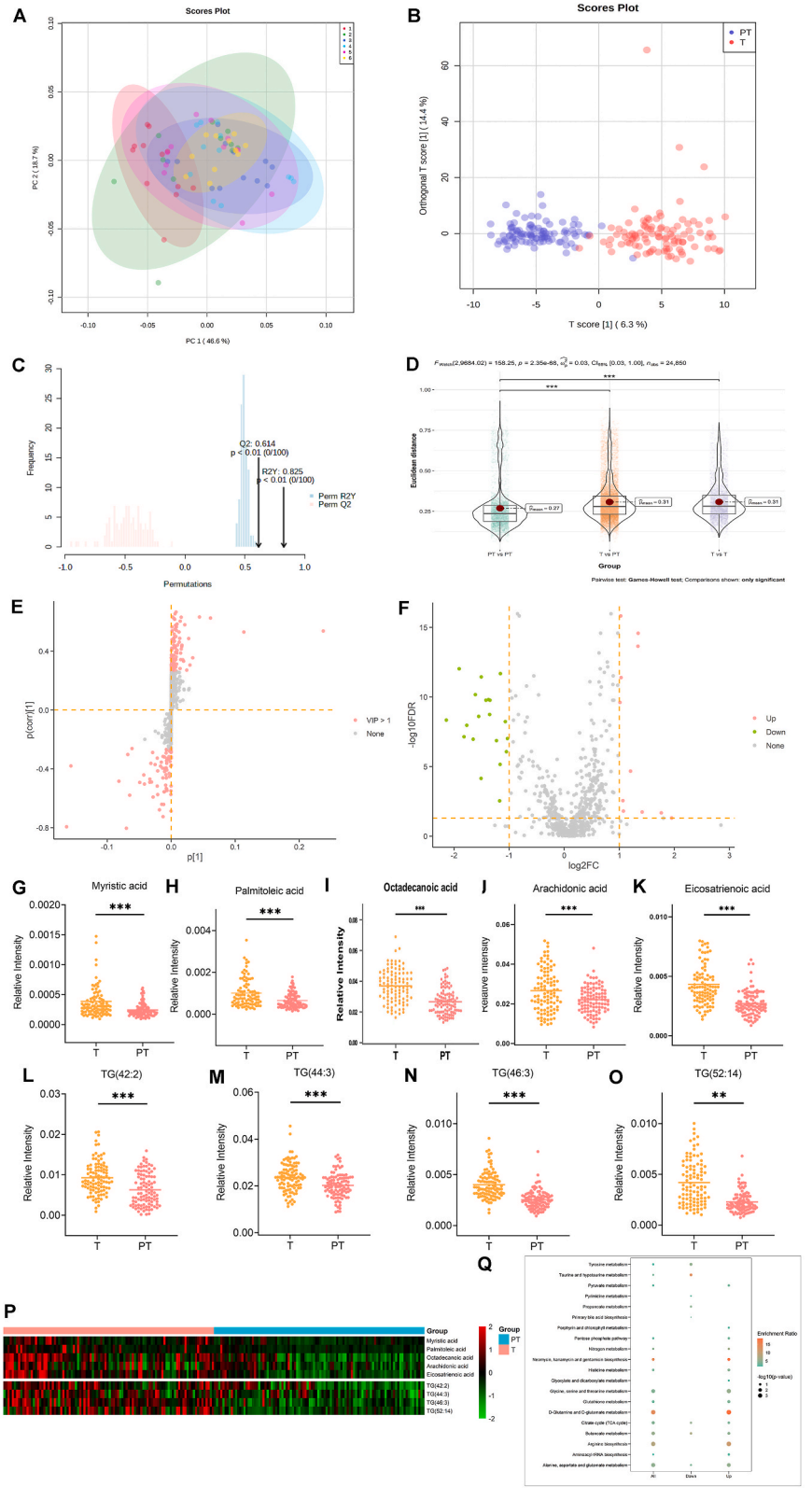

(caption on next page)

Fig. 3. Metabolic dysregulation in GC. a. Principal component analysis of QC samples of each batch. b. OPLS-DA of tumor and paracancerous tissues. c. Permutation test diagram of the OPLS-DA model validation. d. Violin-boxplot constructed using Euclidean distance analysis. e. S-plot analysis of the differential metabolites between tumor and paracancerous tissues. f. Volcano plot of the differential metabolites between tumor and paracancerous tissues. g-k. Comparison of partial differential fatty acid metabolites. l-o. Comparison of partial differential triglyceride metabolites. p. Metabolic heatmap of fatty acids and triglycerides in tumor and paracancerous tissues. q. Enrichment analysis of the differential metabolite pathways in gastric tumor and paracancerous tissues.

expression levels of 4-pyridoxic acid, glucose-6-phosphate, gentisic acid and fumaric acid in Cluster 2 were significantly lower than those in Clusters 1 and 3 ($p < 0.05$), which indicated that carbohydrate metabolism in Cluster 2 was significantly decreased (Fig. 5c). In contrast, the expression levels of ceramide (cer (m42:2)), sphingomyelin (SM(d40:1)), phosphatidylcholine (PC (36:1)) and phosphatidylethanolamine (PE (18:0_18:1)) in Cluster 2 were significantly higher than those in Clusters 1 and 3 ($p < 0.01$), indicating significant lipid accumulation in Cluster 2 (Fig. 5c).

2.2.7. The molecular typing system of GC was established by WES and metabolomics

Inspired by the rich results of GC metabolomics, we also wanted to determine whether there were special metabolic characteristics among the subtypes of the molecular systems established based on WES. First, differential metabolites among subtypes were screened out (Table S25). The enrichment pathways of these differential metabolites were significantly enriched in glycolipid metabolism at the microscopic gene level (Fig. S8). Considering the high heterogeneity of GC and the nonnegligible influence of nongenetic factors, we jointly established a novel molecular typing system for GC by combining WES and metabolomics. First, we used the mogsa package and mbpca function in R to reduce the dimensions of the genomic and metabolomics results to 20 principal components. Then, 100 GC samples were divided into 4 subtypes by unsupervised clustering (Fig. 6a–b). Survival analysis showed significant differences in OS and PFS among the subtypes. Subtype 1 had the best prognosis, followed by subtype 3, subtype 2 had worse prognosis, and subtype 4 had the worst prognosis (Fig. 6c–d). Cox regression analysis supported this conclusion, indicating that this classification system could be used as an independent prognostic factor (Fig. 6e).

Subsequently, we analyzed the correlations between subtypes and clinicopathology and found that subtypes 2 and 4 had a higher proportion of diffuse/mixed tumors, and subtype 4 had a significantly higher proportion of low differentiation and stage III-IV samples than other subtypes (Fig. 6f). Meanwhile, the results of neoantigen analysis showed that the number of neoantigens of subtype 4 was the lowest, while that of subtype 1 was the highest, which was significantly consistent with the results of TMB analysis (Fig. 6g–h). In summary, these results suggest that subtype 4 had the worst prognosis, subtype 1 had the best prognosis, which was highly consistent with the results of survival analysis.

Then, we analyzed the mutation molecular characteristics of the four subtypes. It was found that the mutation frequency of *ARID1A*, the deletion of *LAST1* and *NRAS*, and the amplification ratios of *AXIN1* were higher in Subtype 1, while Subtype 2 had a higher mutation frequency of *MUC16*. In Subtype 3, there were higher mutation frequencies of *TP53* and *FAT3* and higher deletion ratios of *AXIN1* and *RNF43*. In Subtype 4, the deletion ratio of *CTNNB1* was higher (Table 1). Further analysis of specific differential metabolites revealed that the metabolism of subtype 4 was significantly different from those of other subtypes, except that cysteine was highest in subtype 3, and the levels of 4-hydroxyproline, asparagine, N-acetylphenylalanine, 4-D-erythrose phosphate, azelaic acid and 1,7-dimethyluric acid were highest in subtype 4 (Fig. 6i-o, Table S26).

3. Discussion

The tumor heterogeneity of gastric cancer covers a wide range from the microscopic molecular level to the macroscopic apparent characteristics; this heterogeneity leads to drug resistance, cancer recurrence, metastasis and other malignant outcomes [3,11–13]. TCGA cohort classified heterogeneous GC into four molecular subtypes: Epstein-Barr virus positive tumors (EBV), microsatellite instability tumors (MSI), chromosome instability tumors (CIN), and genome stable tumors (GS) [14]. In addition, the Asian Cancer Research Group (ACRG) identified four distinct molecular subtypes associated with survival and postoperative recurrence patterns in GC patients using array-based gene expression profiling: Microsatellite stability/epithelial-mesenchymal transition (MSS/EMT), MSI, MSS/tumor protein 53 activity (MSS/TP53+), and MSS/TP53 inactivation (MSS/TP53-) [15]. However, neither of these classifications were designed to optimize selection of GC patients receiving targeted therapy [16]. In order to adapt to different stress stimuli and meet the needs of rapid proliferation, tumor cells often experience variation in genetic background during their growth and development, and these genetic changes are usually closely related to the level of metabolism. Therefore, it is urgent to establish a molecular classification method for GC at the multidimensional level. In this study, we revealed the genome dynamics and metabolic changes in Chinese GC patients from the perspectives of genomics and metabolomics, respectively; through combined biomics analysis, for the first time, we proposed four GC subtypes that were more complete than those defined in previous studies [8]. These four GC subtypes differ significantly in terms of clinical prognosis, molecular changes and metabolic turnover.

Metabolic reprogramming, a major hallmark of cancer, is closely related to the clinical outcomes and biological characteristics of many cancers [17–20]. In this study, we successfully divided GC into three heterogeneous subtypes with different metabolic and clinicopathological characteristics, and clinical prognoses by employing metabolomics. High glucose demand and anaerobic glycolysis are common metabolic characteristics of cancer cells [21–25]. In harsh living environments lacking sufficient sugar sources and oxygen, tumor cells often use lactic acid and glutamine as alternative carbon sources for accelerated decomposition to maintain energy production and anabolic metabolism [26–29]. This phenomenon is usually accompanied by mutagenic destruction of TCA cycling

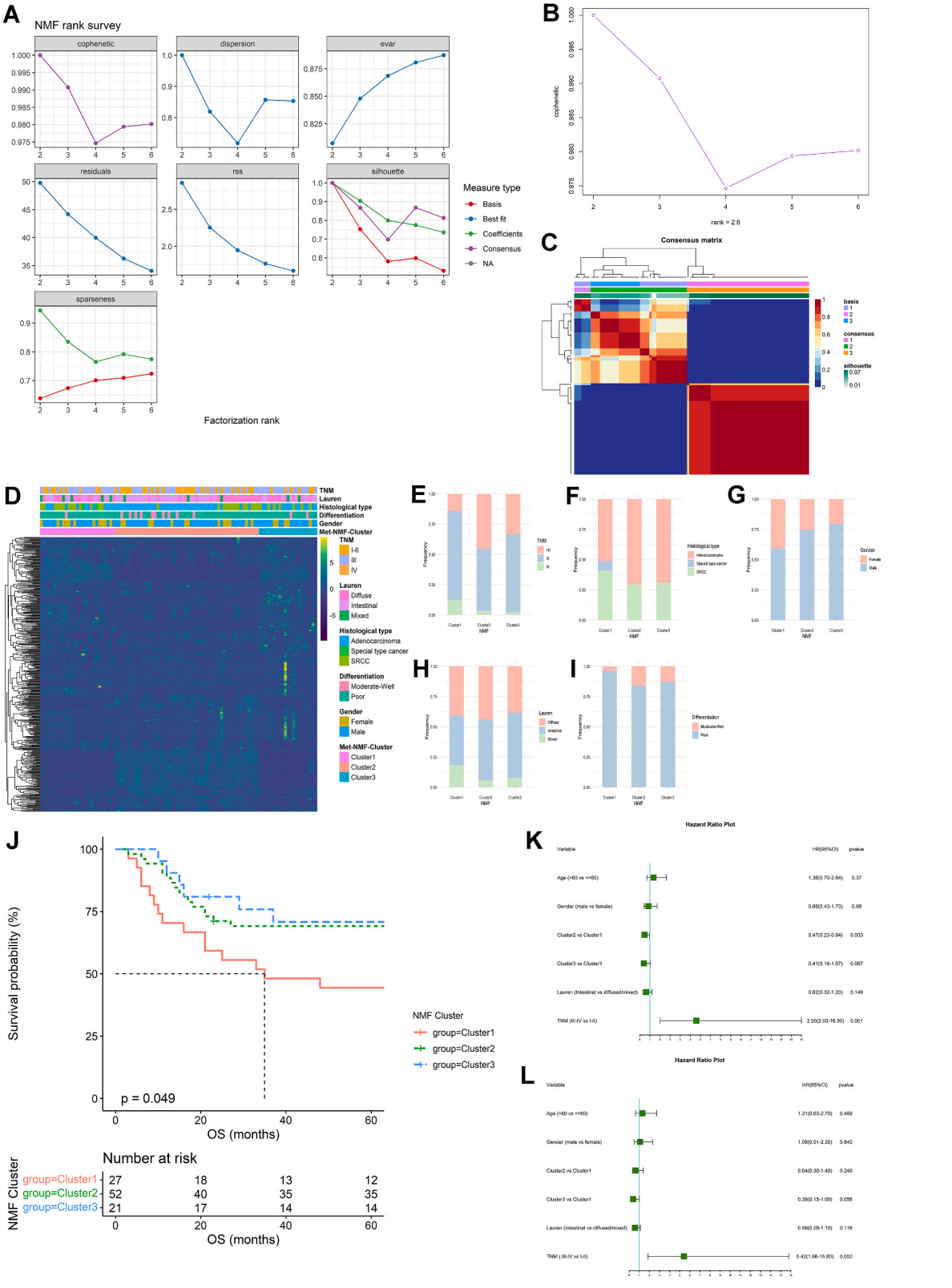

(caption on next page)

Fig. 4. Molecular typing system of gastric cancer established based on metabolomics. a. Nonnegative matrix factorization (NMF) method for unsupervised cluster analysis. b. Decomposition graph with cophenetic as the cluster evaluation indicator. c. Consensus matrix with rank = 3. d. Heatmap of the distribution of clinical features in the three subtypes. e-i. Correlations between different subtypes and histopathology. j. Overall survival curves of the different subtypes. k. Univariate analysis including clinicopathologic features and molecular typing. l. Multivariate analysis including clinicopathologic features and molecular typing.

enzymes [30] and the activation of protein and nucleotide synthesis [31], which promote the conversion of tyrosine, valine and cysteine into TCA intermediates for energy production. We found that subtype 1 patients were mostly stage III-IV patients and had poorer nutritional status than the other two subtypes according to metabolic characteristics, requiring more carbon sources to maintain energy metabolism. In this subtype, amino acid metabolism, carbohydrate metabolism and nucleotide metabolites were upregulated, indicating that cancer cells of this subtype were more aggressive, which might partly explain why subtype 1 had the worst prognosis. The local tumor environment (TME) also plays an important role in cancer cell metabolism [32]. Glutamine decomposition is a key metabolic process in cancer driven by the proto-oncogene *MYC* [29,33]. A previous study showed that the high uptake of glutamine by tumor cells is simultaneously strongly controlled by tumor cells and is involved in the regulation of glucose utilization in the TME [34], which is consistent with our findings that the glutamine metabolism pathway is significantly enriched in cancer tissues. These data also support the application of glutamine metabolism as a specific strategy for inhibiting cancer cell growth.

More interestingly, we found that subtype 2 with a good prognosis showed significant lipid accumulation, while subtype 1 with a poor prognosis showed obvious “glycotropism”, which led us to speculate that there was a unique metabolic selection trend of cancer cells in the TME. Consistent with our findings, previous studies have shown that the sugar uptake of cancer cells accounts for approximately 2/3 of the total glucose uptake in the TME, indicating an obvious preference for glucose [34]. In addition to the study of high glucose supply, the study of fat composition in TME has also deepened our understanding of the heterogeneity of GC. Studies have shown that high lipid levels in the TME can transform macrophages from the M2 type to the M1 type, stimulate the activation and phagocytosis of TLR4-dependent M1 macrophages in adipose tissue, and ultimately prevent the metastasis and spread of colorectal cancer [35]. These effects may partly explain the better prognosis of subtype 2, which is characterized by significant lipid accumulation. In conclusion, the dominant components of metabolic characteristics in different types of metabolomics were different, reflecting the metabolic heterogeneity of Chinese GC and suggesting that comprehensive analyses should be carried out when developing anti-metabolic measures.

Inspired by the metabolic results, we further analyzed the metabolic differences in the transcriptional results and found that glycolipid metabolism was a key enrichment pathway. The high coincidence between the gene and phenotypic levels prompted us to further integrate the results of WES and metabolomics to establish a biomics study. We ultimately successfully divided GC into four subtypes with different metabolic characteristics, genomic alterations, and clinical prognoses. Subtype 1 is considered to be the most promising subtype to benefit from combination immunotherapy, as it is characterized by significant genomic alterations, such as high frequencies of *ARID1A* mutation, *LATS1* deletion, *NRAS* deletion, and *AXIN1* amplification, a high number of neoantigens and TMB. Studies have demonstrated that ARID1A (the AT-rich interaction domain 1A) can interact with the mismatch repair (MMR) protein during DNA replication, and its mutation can impair the MMR process and increase the number of tumor mutations, tumor-infiltrating lymphocytes and PD-L1 expression, ultimately sensitizing immunotherapy [36–40]. These results were consistent with the characteristic changes in subtype 1, suggesting that the development of targeted therapy for *ARID1A* mutations is very reasonable to improve the efficacy of clinical immunotherapy. This is in agreement with the recent report by Xu et al. [41]. Subtype 2 was associated with a high frequency *MUC16* mutation. Given the potential positive promoting effect of high mutation frequency of *MUC16* on immunotherapy [42–44], this provided a certain theoretical basis for the selection of immunotherapy in subtype 2 patients. Significant upregulation of cysteine was observed in subtype 3, accompanied by high frequencies of *TP53* mutation, *FAT3* mutation, *AXIN1* deletion, and *RNF43* deletion. It has been reported that when cysteine supply to tumors is cut off by knockout of the gene controlling cysteine input, tumor growth is significantly restarted, and cysteine depletion causes a large increase in lipid oxidation, inducing the process of ferroptosis and promoting the further apoptosis of tumor cells [45,46]. More importantly, most normal cells have a low requirement for cysteine [47], while cancer cells depend on cysteine. This significant difference makes targeted cysteine therapy an important breakthrough to correct metabolic disorders in cancer. The metabolic characteristics that distinguish subtype 3 from the other subtypes may enable patients with this subtype to benefit greatly from anti-cysteine metabolic therapy.

Subtype 4 included the most advanced patients, with the worst immunogenicity and nutritional status and the poorest prognosis. In terms of metabolism, we found that the expression levels of 4-hydroxyproline, asparagine, N-acetylphenylalanine, 4-D-erythrose phosphate, azelaic acid, and 1,7-dimethyluric acid were generally upregulated. In other words, the level of amino acid metabolism of subtype 4 was extremely high, which was similar to the characteristics of metabolic subtype 1, suggesting that the adverse TME, characterized by nutrient deficiency and hypoxia, might accelerate the intake of alternative carbon sources and promote the occurrence of adverse outcomes. For example, the amino acid asparagine is required for protein synthesis [29,48], though blocking asparagine does not lead to tumor cell death. However, tumor cells activate the MAPK pathway, allowing cancer cells to produce asparagine on their own [49,50]. Studies have shown that the combination of MEK inhibitors and asparagine blockers can inhibit tumor growth and metastasis in an effective dose-dependent manner [50]. Therefore, amino acid-blocking therapy is considered a potential anticancer strategy. In terms of gene alteration, subtype 4 was accompanied by a high frequency of *CTNNB1* deletion. It is well known that β-catenin, the main downstream effector molecule in the classical Wnt signaling pathway, is encoded by *CTNNB1* (cadherin-associated protein beta-1). Deletion or mutation of *CTNNB1* can affect the activity of the β-catenin protein, thus activating the Wnt/β-catenin signaling pathway and promoting the malignant phenotype of tumors [51–53]. In addition, a multiomics analysis of

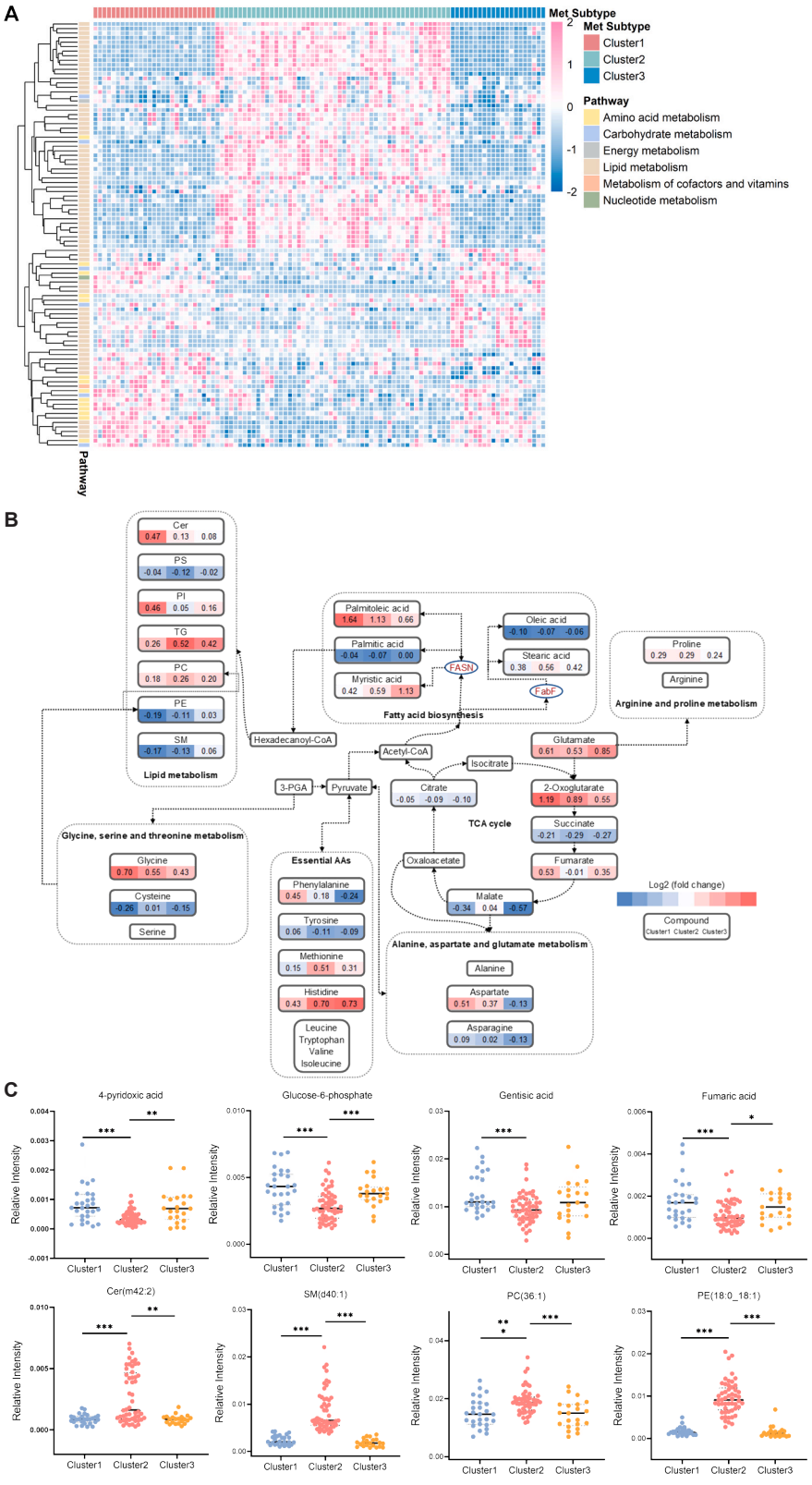

Fig. 5. GC molecular typing system based on metabolomics with different metabolic features among subtypes. a. Heatmap of the metabolic characteristics of the three subtypes. b. Metabolic overview of the three subtypes, including carbohydrate metabolism, amino acid metabolism, fatty acid biosynthesis, and lipid metabolism. c. Expression levels of typical metabolites between the three subtypes.

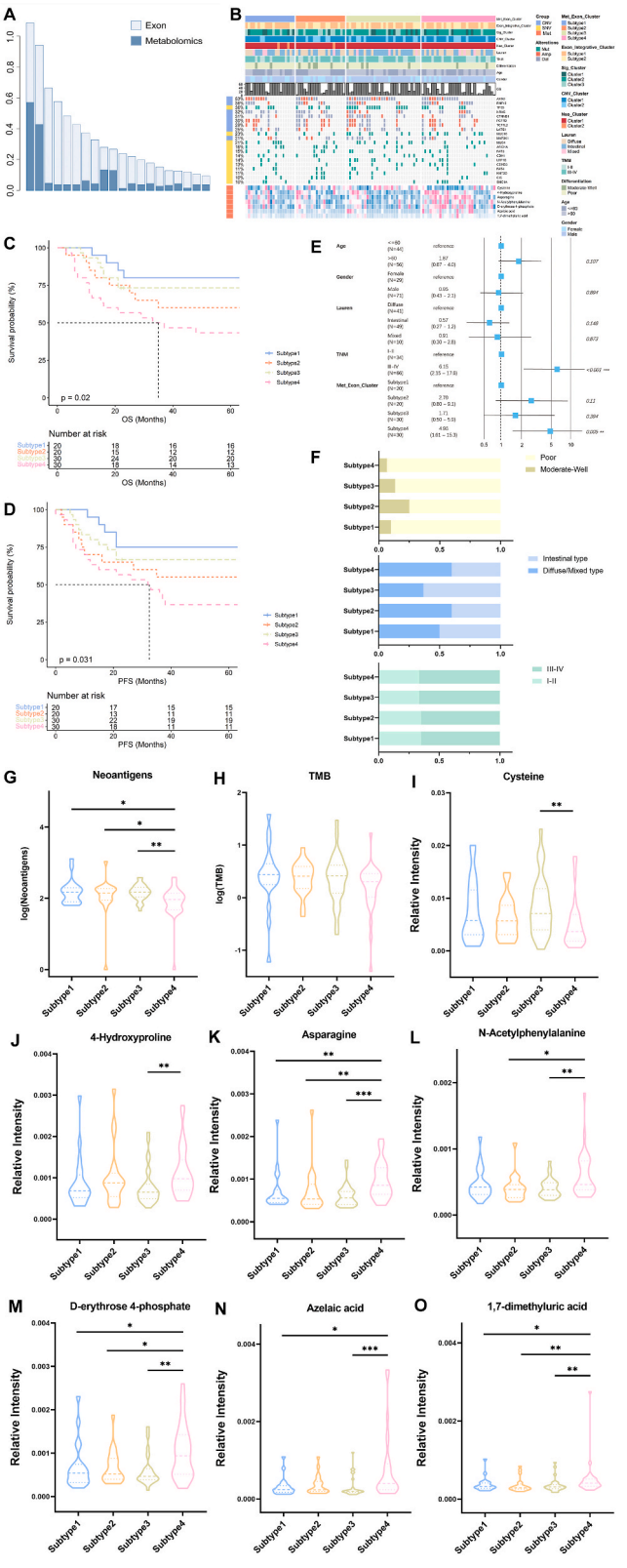

(caption on next page)

Fig. 6. Molecular typing system of GC established based on WES and metabolomics. a. Dimensionalities of the genome integration and metabolomics results reduced to 20 principal components by the mbpca function in the mogsa package in R. b. Unsupervised clustering results of 20 principal components. One hundred GC samples were divided into 4 subtypes: the top shows the distribution of other subtypes and clinical features, the middle shows SNV and CNV features, and the bottom shows metabolic molecules with significant ($p < 0.05$) differences among the 4 subtypes tested by Kruskal-Wallis analysis. c. Comparison of the overall survival (OS) curves among the different subtypes. d. Comparison of the progression-free survival (PFS) curves among the different subtypes. e. Multivariate COX regression analysis involving clinicopathologic features and molecular typing. f. Bar charts of the distribution ratios of the clinical features in each subtype. g. Violin plot of the neoantigens in each subtype. h. Violin plot of TMB in each subtype. i-o. Differential metabolite analysis of the biomics-based molecular typing system. *$p < 0.05$; **$p < 0.01$; ***$p < 0.001$.

Table 1
Molecular characteristics of mutations in each subtype of the biomics-based molecular typing system.

ID		Subtype1	Subtype2	Subtype3	Subtype4	p.value
TP53	mutation	30 %	30 %	**40 %**	37 %	0.912264
MUC16	mutation	15 %	**40 %**	23 %	17 %	0.201738
MUC4	mutation	15 %	15 %	27 %	23 %	0.674986
ARID1A	mutation	**30 %**	15 %	17 %	7 %	0.184125
FAT3	mutation	5 %	25 %	**30 %**	0 %	***0.003523***
CDH1	mutation	25 %	20 %	7 %	10 %	0.230535
LRP1B	mutation	15 %	20 %	23 %	0 %	0.055236
CSMD3	mutation	20 %	15 %	13 %	7 %	0.575717
FAT4	mutation	10 %	0 %	23 %	7 %	0.053786
KMT2D	mutation	20 %	10 %	13 %	3 %	0.30718
CIC	mutation	10 %	15 %	7 %	10 %	0.821404
SMC1A	mutation	10 %	20 %	13 %	0 %	0.11828
AXIN1	deletion	35 %	30 %	**40 %**	23 %	0.568885
CTNNB1	deletion	25 %	30 %	13 %	**33 %**	0.318177
FGFR2	deletion	10 %	15 %	13 %	7 %	0.78223
LATS1	deletion	**30 %**	5 %	7 %	23 %	0.050705
MAP2K1	deletion	20 %	10 %	20 %	13 %	0.734653
NRAS	deletion	**40 %**	30 %	30 %	0 %	***0.003719***
RNF43	deletion	15 %	25 %	**43 %**	13 %	***0.036141***
TCF7L2	deletion	10 %	15 %	13 %	10 %	0.938948
AXIN1	amplification	**30 %**	20 %	17 %	20 %	0.721376
CTNNB1	amplification	10 %	5 %	7 %	3 %	0.802539
FGFR2	amplification	5 %	20 %	27 %	20 %	0.297172
LATS1	amplification	0 %	15 %	10 %	10 %	0.407126
MAP2K1	amplification	10 %	5 %	0 %	7 %	0.426977
NRAS	amplification	0 %	5 %	10 %	17 %	0.21115
RNF43	amplification	10 %	10 %	10 %	13 %	0.971586
TCF7L2	amplification	10 %	15 %	23 %	17 %	0.661577

1The ***italicized and bold*** represent significantly different molecules between subtypes.
2The **underscore and bold** represents mutation frequency ≥30 % and is the highest mutation frequency among the four subtypes.

hepatocellular carcinoma (HCC) showed that protein enrichment in *CTNNB1*-mutated tumors is associated with a variety of metabolic processes, including glycolysis and amino acid metabolism, suggesting that CTNNB1 activation may influence the metabolic reprogramming of HCC cells at the translational and posttranslational levels [54]. Therefore, it would be wise to conduct research on β-catenin or upstream and downstream signaling proteins. Given the low immunogenicity of subtype 4, we suggest that a combination of amino acid-blocking therapy and β-catenin inhibitors might constitute a more comprehensive treatment.

Note here that our research group previously constructed a molecular system named ZJU-GC [8] based on the WES results of 70 gastric cancer cases. The research group continued to expand this sample and added another dimension of omics analysis to improve the understanding of the heterogeneity of gastric cancer at the multimolecular level. However, there are still shortcomings in our research. First, the results of drug sensitivity experiments were not included in this study to verify the effectiveness of corresponding metabolic inhibitors or target inhibitors against each subtype; these trials are currently being carried out in our laboratory. Second, this was a single-center retrospective study, which lacked the validation of a large multicenter cohort study. Therefore, it will be necessary to conduct further studies to verify potential target molecules and driving factors in the future and to conduct multicenter prospective trials to consolidate the clinical significance of the molecular typing system.

4. Conclusions

This multidimensional analysis reveals the genomic characteristics and unique metabolic manifestations of Chinese gastric cancer patients and establishes a new set of molecular systems, enriching our understanding of the heterogeneity of gastric cancer in China. Although the results of our study need further biological validation and clinical verification, they have certain implications for the understanding of the changes in gastric cancer metabolism and the development of new targets in the future.

5. Material and methods

5.1. Collection of patient tissue samples

In this study, we included 100 patients with pathologically confirmed GC who underwent radical gastrectomy in the First Affiliated Hospital of Zhejiang University College of Medicine from January 2016 to January 2018. Some of the patients were from the previous study cohort [8], so they were also named ZJU-GC. The criteria for study inclusion were as follows: patients aged 18–85 years; the imaging and pathological diagnosis was GC on admission; the patient underwent surgical treatment in our hospital, and the clinical data were complete; postoperative pathology confirmed GC with negative incisional margins; there was no other primary tumor; and there was no infectious disease or acute or chronic infection. This study was approved by the Ethics Committee of the First Affiliated Hospital of Zhejiang University School of Medicine.

5.2. Exon sequencing

5.2.1. DNA extraction

DNA was extracted from 100 pairs of gastric cancer and adjacent tissues. Genomic DNA was isolated using the QIAamp DNA Mini Kit (Qiagen). After verifying the quality of the isolated genomic DNA, DNA samples with a concentration of $\geq$20 ng/μL and a total amount of 0.4 μg or more were used for library construction.

5.2.2. Whole-exome sequencing

The genomic DNA was randomly fragmented by a Covaris fragmentation instrument to a length of 180–280 bp. A whole-exon library was constructed using an Agilent SureSelect Human All Exon V6 Kit (Agilent Technologies, Santa Clara, CA, USA). The index-coded sample was classified on a cBot Cluster Generation System using a HiSeq PE Cluster Kit (Illumina). The DNA library was then sequenced on the Illumina HiSeq platform (Illumina, San Diego, California, USA), and paired-end reads of 150 bp were generated. Data quality control was performed first, followed by all downstream bioinformatics analyses based on high-quality clean data. The paired-ended clean reads were aligned with reference genome build 37 (GRCh37) using BWA v.0.7.8. SAMtools was used to sort the results [55]. Then, the duplicate reads were marked with Sambamba. Finally, the comparison results after repeated labeling were used to calculate the coverage and depth.

5.2.3. Somatic mutation detection and identification of significant mutant genes

Somatic single-nucleotide variants (SNVs) were identified by Mutect (v 1.1.4), and somatic InDels were detected by Strelka (v1.0.13). ANNOVAR (ANNOVAR_2015Mar22) was used to annotate the variant call format file. The Mutational Significance in Cancer (Music, version: Genome-Model-Tools-Music-0.04) algorithm was used to identify significantly mutated genes (SMGS) from profiles of somatic SNVS and InDels (false discovery rate (FDR) $<$ 0.25).

5.2.4. Mutation characteristic analysis

Mutations were characterized according to the 96-substitution classification. Based on the frequencies of 96 mutation types, a nonnegative matrix decomposition (NMF) method was performed using the maftools package to extract the mutation signatures and compare them with the known signatures cited in the Cancer Somatic Mutation Catalog and the 96-Substitution Classification (COSMIC) database. Cosine similarity $>$0.9 evaluated the similarity of mutation features and regarded those with cosine similarity $>$0.9 as common features. Then, unsupervised hierarchical clustering was carried out to identify the subtype of the mutant feature (Sig_cluster) according to the proportional contribution of each signature of each sample.

5.2.5. Copy number analysis

Somatic cell copy number variation (SCNV) was identified using CNVkit. Then, GISTIC 2.0 (v 2.0.22) was used to identify significantly altered genomic regions and screen out relapsed CNV regions (parameters: rx 0-ext xls-fname ALL-ta 0.1-td 0.1-js 4-qvt 0.25-cap 1.5-board 1-maxseg 2000-conf 0.99-genegistic 1 -armpeel 1-brlen 0.7 -gcmextreme-savegene 1). In addition, unsupervised hierarchical clustering was performed to identify copy number variant subtypes (CNV_cluster) based on discrete CNVs.

5.2.6. HLA genotyping and neonatal antigen prediction

WES raw data were processed using TSNAD software. After identifying somatic mutations, TSNAD was used to determine HLA genotyping via SOAP-HLA. NetMHCpan was then called to predict mutation-derived neoantigens that could bind to Class I MHC molecules. Then, unsupervised hierarchical clustering was performed to identify the classification of newborn antigens according to the number of neoantigens (Neo_cluster).

6. Metabolomics

6.1. Metabolite extraction

Approximately 25 mg of each sample was placed in a 1.5 mL centrifuge tube, and 150 μL ultrapure water was added for grinding. Then, the sample was mixed evenly with vortex oscillation so that the ground tissue became liquid. A total of 150 μL was taken from

each sample and added to the centrifuge tube. Each well was supplemented with 84 μL methanol, 416 μL methyl *tert*-butyl ether and 150 μL ultrapure water, and the sample was centrifuged after oscillation. The upper layer of 150 μL and the lower layer of 300 μL liquid were dried at room temperature, 100 μL IPA/H2O [3/1] was added to the upper layer of the dried sample to suspend it, and the resulting suspension was then vortexed for 10s. After drying, 260 μL ACN/MeOH/H2O [1.5/1.5/1] was added to the lower layer to suspend the sample, which was then ultrasonically treated for 5s and vortexed for 10 s. The upper layer of 10 μL and the lower layer of 30 μL of the resuspension vortex were mixed by vortex for 10 s.

6.1.1. Metabolite detection

A 1 μL sample was deposited onto a Met-Si Array® chip (Well-health care Technologies Co., Ltd.), which contains arrays of vertical silicon nanowire structures [56–58]. Then, the chip was placed on a custom-made plate and inserted into an Autoflex Max MALDI-TOF/TOF mass spectrometer (Bruker Daltonics Inc.) for metabolite and lipid profiling.

6.1.2. Metabolomics data analysis

Flexanalysis 3.4 (Bruker Daltonics Inc.) was used to export the original data in txt format. Data cleaning and peak alignment were performed using HJ Cloud MDAS PreData 2.40. The decostand function in the vegan package of R was used for data normalization. The dist function of R was used to calculate the European distances between samples to determine the differences in metabolites between gastric cancer and adjacent tissues. Orthogonal partial least squares discriminant analysis (OPLS-DA) and differential metabolite path set enrichment were analyzed using the MetaboAnalystR package in R. Using R language, the nsNMF method of the NMF package was used to perform unsupervised clustering to identify metabolome subtypes. Kaplan–Meier survival curve analysis and Cox function univariate and multivariate risk regression analyses were performed using the R survival and survminer packages to predict the factors that might affect patient prognosis.

6.1.3. Integrated cluster analysis

Molecular subtypes, including Sig_Cluster, CNV_Cluster, Neo_Cluster, SMG and CNV, were revealed based on the characteristics of multiple genomes. SMGs were selected with the overlap between the genes with a mutation frequency $\geq$10 % in our cohort and the cancer-related genes in COSMIC [59]. CNV genes with a change frequency $\geq$10 % and with a relation to cancer in COSMIC were selected. Then, the mbpca function in the mogsa package in R (version 4.1.3) reduced the genome mutation characteristics, Sig-cluster, CNV-cluster, The unsupervised clustering method of the iClusterPlus package was used for clustering. The values of these variables are shown in Table S1.

6.1.4. Statistical analysis

All statistical analyses were performed in R 4.1.3, and differences between categorical variables were compared by the chi-square test or Fisher's exact test. Nonparametric variables were evaluated by the Mann–Whitney test. Survival data were analyzed by Kaplan–Meier curves and log-rank tests. Hazard ratios (95 % confidence intervals) were calculated by univariate and multivariate Cox regression analyses. A p value < 0.05 was considered significant.

Data availability

The raw sequence data reported in this paper have been deposited in the Genome Sequence Archive (Genomics, Proteomics & Bioinformatics 2021) in National Genomics Data Center (Nucleic Acids Res 2022), China National Center for Bioinformation/Beijing Institute of Genomics, Chinese Academy of Sciences (GSA-Human: HRA006984) that are publicly accessible at https://ngdc.cncb.ac.cn/gsa-human.

Funding

This study was funded by Key Research and Development Program of Science and Technology Department of Zhejiang Province (No. 2020C03112 to D.Z.) and National Natural Science Foundation of China (No. 82072631 to D.Z.).

Ethical approval

All procedures were conducted in accordance with the ethical standards of the corresponding committees on human experimentation (institutional and national) and with the Helsinki Declaration of 1964 and later versions. This study was approved by the ethics committee of the First Affiliated Hospital of Zhejiang University School of Medicine (No. 2020-365).

Informed consent

Informed consent was obtained from all patients included in the study.

CRediT authorship contribution statement

Shanshan Yu: Writing – review & editing, Writing – original draft, Software, Formal analysis. **Ming Chen:** Writing – review &

editing, Writing – original draft, Formal analysis. **Xiaohua Zhu:** Writing – review & editing, Writing – original draft, Methodology, Data curation. **Cheng Chen:** Methodology, Data curation. **Jinxiao Liang:** Methodology, Data curation. **Haiyong Wang:** Conceptualization. **Jun Lu:** Software, Methodology, Data curation. **Yongfeng Ding:** Software, Methodology, Data curation. **Mei Kong:** Formal analysis. **Lisong Teng:** Conceptualization. **Donghui Zhou:** Writing – review & editing, Funding acquisition, Conceptualization.

Declaration of competing interest

The authors declare that they have no known competing financial interests or personal relationships that could have appeared to influence the work reported in this paper.

Acknowledgements

The authors sincerely thank the assistance of bioinformatics analyses from Well-healthcare Technologies Co. Ltd., Hangzhou, China.

Appendix A. Supplementary data

Supplementary data to this article can be found online at https://doi.org/10.1016/j.heliyon.2024.e34317.

References

[1] H. Sung, J. Ferlay, R. Siegel, M. Laversanne, I. Soerjomataram, A. Jemal, et al., Global cancer statistics 2020: GLOBOCAN estimates of incidence and mortality worldwide for 36 cancers in 185 countries, Ca - Cancer J. Clin. 71 (3) (2021) 209–249.
[2] C. Allemani, T. Matsuda, V. Di Carlo, R. Harewood, M. Matz, M. Nikšić, et al., Global surveillance of trends in cancer survival 2000-14 (CONCORD-3): analysis of individual records for 37 513 025 patients diagnosed with one of 18 cancers from 322 population-based registries in 71 countries, Lancet (London, England) 391 (10125) (2018) 1023–1075.
[3] C.G.A.R. Network, Comprehensive molecular characterization of gastric adenocarcinoma, Nature 513 (7517) (2014) 202–209.
[4] R. Taylor, A. Pyle, H. Griffin, E. Blakely, J. Duff, L. He, et al., Use of whole-exome sequencing to determine the genetic basis of multiple mitochondrial respiratory chain complex deficiencies, JAMA 312 (1) (2014) 68–77.
[5] Y. Ng, C. Alston, D. Diodato, A. Morris, N. Ulrick, S. Kmoch, et al., RMND1The clinical, biochemical and genetic features associated with -related mitochondrial disease, J. Med. Genet. 53 (11) (2016) 768–775.
[6] J. Casey, E. Crushell, K. Thompson, E. Twomey, L. He, S. Ennis, et al., Periventricular calcification, abnormal pterins and dry thickened skin: expanding the clinical spectrum of RMND1? JIMD reports 26 (2016) 13–19.
[7] S. Tay, S. Leong, K. Yu, A. Aggarwal, S. Tan, C. Lee, et al., A combined comparative genomic hybridization and expression microarray analysis of gastric cancer reveals novel molecular subtypes, Cancer Res. 63 (12) (2003) 3309–3316.
[8] H. Wang, Y. Ding, Y. Chen, J. Jiang, Y. Chen, J. Lu, et al., A novel genomic classification system of gastric cancer via integrating multidimensional genomic characteristics, Gastric Cancer 24 (6) (2021) 1227–1241.
[9] H. Abbiss, G. Maker, R. Trengove, Metabolomics approaches for the diagnosis and understanding of kidney diseases, Metabolites 9 (2) (2019).
[10] R. Shrestha, N. Nabavi, Y. Lin, F. Mo, S. Anderson, S. Volik, et al., BAP1 haploinsufficiency predicts a distinct immunogenic class of malignant peritoneal mesothelioma, Genome Med. 11 (1) (2019) 8.
[11] N. McGranahan, C. Swanton, Biological and therapeutic impact of intratumor heterogeneity in cancer evolution, Cancer Cell 27 (1) (2015) 15–26.
[12] A. Marusyk, M. Janiszewska, K. Polyak, Intratumor heterogeneity: the rosetta stone of therapy resistance, Cancer Cell 37 (4) (2020) 471–484.
[13] N. McGranahan, C. Swanton, Clonal heterogeneity and tumor evolution: past, present, and the future, Cell 168 (4) (2017) 613–628.
[14] T. Toshiaki, T. Hiroaki, M. Yoshiko, T. Takehiro, Y. Kazuya, K. Keisuke, et al., Genomically stable gastric cancer characterized by hypomethylation in Wnt signal cascade, Oncology 101 (2) (2022).
[15] Z. Haoran, Z. Shuman, D. Pingan, T. Bibo, W. Hongyan, L. Wenbo, et al., Screening of differentially expressed genes based on the ACRG molecular subtypes of gastric cancer and the significance and mechanism of AGTR1 gene expression, J Pers Med 13 (3) (2023).
[16] I. Hiroshi, N. Masayuki, S. Yoshifumi, H. Takaaki, I. Takashi, K. Hitoshi, et al., Actionable gene-based classification toward precision medicine in gastric cancer, Genome Med. 9 (1) (2017).
[17] G. Gentric, Y. Kieffer, V. Mieulet, O. Goundiam, C. Bonneau, F. Nemati, et al., PML-regulated mitochondrial metabolism enhances chemosensitivity in human ovarian cancers, Cell Metabol. 29 (1) (2019), 156-73.e10.
[18] Y. Gong, P. Ji, Y. Yang, S. Xie, T. Yu, Y. Xiao, et al., Metabolic-pathway-based subtyping of triple-negative breast cancer reveals potential therapeutic targets, Cell Metabol. 33 (1) (2021) 51–64.e9.
[19] Y. Tan, J. Li, G. Zhao, K. Huang, H. Cardenas, Y. Wang, et al., Metabolic reprogramming from glycolysis to fatty acid uptake and beta-oxidation in platinum-resistant cancer cells, Nat. Commun. 13 (1) (2022) 4554.
[20] B. Faubert, A. Solmonson, R. DeBerardinis, Metabolic reprogramming and cancer progression, Science (New York, NY) 368 (6487) (2020).
[21] L. Gerace, Molecular trafficking across the nuclear pore complex, Curr. Opin. Cell Biol. 4 (4) (1992) 637–645.
[22] Y. Wang, E. Stancliffe, R. Fowle-Grider, R. Wang, C. Wang, M. Schwaiger-Haber, et al., Saturation of the mitochondrial NADH shuttles drives aerobic glycolysis in proliferating cells, Mol Cell 82 (17) (2022), 3270-83.e9.
[23] K. Johnston, P. Pachnis, A. Tasdogan, B. Faubert, L. Zacharias, H. Vu, et al., Isotope tracing reveals glycolysis and oxidative metabolism in childhood tumors of multiple histologies, Med (New York, NY) 2 (4) (2021) 395–410.
[24] D. Hanahan, R. Weinberg, Hallmarks of cancer: the next generation, Cell 144 (5) (2011) 646–674.
[25] M. Vander Heiden, L. Cantley, C. Thompson, Understanding the Warburg effect: the metabolic requirements of cell proliferation, Science (New York, NY) 324 (5930) (2009) 1029–1033.
[26] J. Doherty, J. Cleveland, Targeting lactate metabolism for cancer therapeutics, J. Clin. Invest. 123 (9) (2013) 3685–3692.
[27] J. Kamphorst, M. Chung, J. Fan, J. Rabinowitz, Quantitative analysis of acetyl-CoA production in hypoxic cancer cells reveals substantial contribution from acetate, Cancer Metabol. 2 (2014) 23.
[28] Z. Schug, B. Peck, D. Jones, Q. Zhang, S. Grosskurth, I. Alam, et al., Acetyl-CoA synthetase 2 promotes acetate utilization and maintains cancer cell growth under metabolic stress, Cancer Cell 27 (1) (2015) 57–71.
[29] D. Wise, C. Thompson, Glutamine addiction: a new therapeutic target in cancer, Trends Biochem. Sci. 35 (8) (2010) 427–433.

[30] A. King, M. Selak, E. Gottlieb, Succinate dehydrogenase and fumarate hydratase: linking mitochondrial dysfunction and cancer, Oncogene 25 (34) (2006) 4675–4682.
[31] J. Hu, J. Locasale, J. Bielas, J. O'Sullivan, K. Sheahan, L. Cantley, et al., Heterogeneity of tumor-induced gene expression changes in the human metabolic network, Nat. Biotechnol. 31 (6) (2013) 522–529.
[32] E. Armitage, A. Southam, Monitoring cancer prognosis, diagnosis and treatment efficacy using metabolomics and lipidomics. Metabolomics, Official journal of the Metabolomic Society 12 (9) (2016) 146.
[33] W. Liu, A. Le, C. Hancock, A. Lane, C. Dang, T. Fan, et al., Reprogramming of proline and glutamine metabolism contributes to the proliferative and metabolic responses regulated by oncogenic transcription factor c-MYC, Proc. Natl. Acad. Sci. U.S.A. 109 (23) (2012) 8983–8988.
[34] B. Reinfeld, M. Madden, M. Wolf, A. Chytil, J. Bader, A. Patterson, et al., Cell-programmed nutrient partitioning in the tumour microenvironment, Nature 593 (7858) (2021) 282–288.
[35] W. Xiang, R. Shi, D. Zhang, X. Kang, L. Zhang, J. Yuan, et al., Dietary fats suppress the peritoneal seeding of colorectal cancer cells through the TLR4/Cxcl10 axis in adipose tissue macrophages, Signal Transduct. Targeted Ther. 5 (1) (2020) 239.
[36] B. Wilson, C. Roberts, SWI/SNF nucleosome remodellers and cancer, Nat. Rev. Cancer 11 (7) (2011) 481–492.
[37] J. Wu, C. Roberts, ARID1A mutations in cancer: another epigenetic tumor suppressor? Cancer Discov. 3 (1) (2013) 35–43.
[38] J. Shen, Z. Ju, W. Zhao, L. Wang, Y. Peng, Z. Ge, et al., ARID1A deficiency promotes mutability and potentiates therapeutic antitumor immunity unleashed by immune checkpoint blockade, Nat. Med. 24 (5) (2018) 556–562.
[39] G. Hu, W. Tu, L. Yang, G. Peng, L. Yang, ARID1A deficiency and immune checkpoint blockade therapy: from mechanisms to clinical application, Cancer Lett. 473 (2020) 148–155.
[40] S. Jones, M. Li, D. Parsons, X. Zhang, J. Wesseling, P. Kristel, et al., Somatic mutations in the chromatin remodeling gene ARID1A occur in several tumor types, Hum. Mutat. 33 (1) (2012) 100–103.
[41] X. Chang, H. Kie Kyon, Hao L. Jia, C. Joy Shijia, S. Taotao, M.F. Natasha, et al., Comprehensive molecular phenotyping of ARID1A-deficient gastric cancer reveals pervasive epigenomic reprogramming and therapeutic opportunities, Gut 72 (9) (2023).
[42] L. Zhang, X. Han, Y. Shi, Association of MUC16 mutation with response to immune checkpoint inhibitors in solid tumors, JAMA Netw. Open 3 (8) (2020) e2013201.
[43] X. Li, B. Pasche, W. Zhang, K. Chen, Association of MUC16 mutation with tumor mutation load and outcomes in patients with gastric cancer, JAMA Oncol. 4 (12) (2018) 1691–1698.
[44] M. Lawrence, P. Stojanov, P. Polak, G. Kryukov, K. Cibulskis, A. Sivachenko, et al., Mutational heterogeneity in cancer and the search for new cancer-associated genes, Nature 499 (7457) (2013) 214–218.
[45] J. Wu, S. Yeung, S. Liu, A. Qdaisat, D. Jiang, W. Liu, et al., Cyst(e)ine in nutrition formulation promotes colon cancer growth and chemoresistance by activating mTORC1 and scavenging ROS, Signal Transduct. Targeted Ther. 6 (1) (2021) 188.
[46] M. Badgley, D. Kremer, H. Maurer, K. DelGiorno, H. Lee, V. Purohit, et al., Cysteine depletion induces pancreatic tumor ferroptosis in mice, Science (New York, NY) 368 (6486) (2020) 85–89.
[47] H. Sato, A. Shiiya, M. Kimata, K. Maebara, M. Tamba, Y. Sakakura, et al., Redox imbalance in cystine/glutamate transporter-deficient mice, J. Biol. Chem. 280 (45) (2005) 37423–37429.
[48] B. Altman, Z. Stine, C. Dang, From Krebs to clinic: glutamine metabolism to cancer therapy, Nat. Rev. Cancer 16 (11) (2016) 749.
[49] M. Thiaville, Y. Pan, A. Gjymishka, C. Zhong, R. Kaufman, M. Kilberg, MEK signaling is required for phosphorylation of eIF2alpha following amino acid limitation of HepG2 human hepatoma cells, J. Biol. Chem. 283 (16) (2008) 10848–10857.
[50] G. Pathria, J. Lee, E. Hasnis, K. Tandoc, D. Scott, S. Verma, et al., Translational reprogramming marks adaptation to asparagine restriction in cancer, Nat. Cell Biol. 21 (12) (2019) 1590–1603.
[51] A. Adebayo Michael, S. Ko, J. Tao, A. Moghe, H. Yang, M. Xu, et al., Inhibiting glutamine-dependent mTORC1 activation ameliorates liver cancers driven by β-catenin mutations, Cell Metabol. 29 (5) (2019), 1135-50.e6.
[52] J. He, Z. Zeng, Y. Wang, J. Deng, X. Tang, F. Liu, et al., Characterization of novel CTNNB1 mutation in Craniopharyngioma by whole-genome sequencing, Mol. Cancer 20 (1) (2021) 168.
[53] F. Liu, X. Gai, Y. Wu, B. Zhang, X. Wu, R. Cheng, et al., Oncogenic β-catenin stimulation of AKT2-CAD-mediated pyrimidine synthesis is targetable vulnerability in liver cancer, Proc. Natl. Acad. Sci. U.S.A. 119 (39) (2022) e2202157119.
[54] Q. Gao, H. Zhu, L. Dong, W. Shi, R. Chen, Z. Song, et al., Integrated proteogenomic characterization of HBV-related hepatocellular carcinoma, Cell 179 (2) (2019), 561-77.e22.
[55] H. Li, B. Handsaker, A. Wysoker, T. Fennell, J. Ruan, N. Homer, et al., The sequence alignment/map format and SAMtools, Bioinformatics 25 (16) (2009) 2078–2079.
[56] X. Chen, T. Wang, L. Lin, F. Wo, Y. Liu, X. Liang, et al., Tip-enhanced photoinduced electron transfer and ionization on vertical silicon nanowires, ACS Appl. Mater. Interfaces 10 (17) (2018) 14389–14398.
[57] T. Wang, X. Chen, C. Luan, J. Wu, High throughput lipid profiling for subtype classification of hepatocellular carcinoma cell lines and tumor tissues, Anal. Chim. Acta 1107 (2020) 92–100.
[58] X. Qu, T. Wang, X. Liu, X. Jiang, X. Liang, J. Wu, Dual-mechanism-driven strategy for high-coverage detection of serum lipids on a novel SALDI-MS target, Anal. Chem. 94 (24) (2022) 8570–8579.
[59] J. Tate, S. Bamford, H. Jubb, Z. Sondka, D. Beare, N. Bindal, et al., COSMIC: the catalogue of somatic mutations in cancer, Nucleic Acids Res. 47 (2019) D941–D947.